ISSN 1674-1056
http://cpb.iphy.ac.cn
http://iopscience.iop.org/cpb
中国物理 B
Chinese Physics
中国物理
Chinese Physics B

X-ray emission for Ar^{11+} ions impacting on various targets in the collisions near the Bohr velocity

Xian-Ming Zhou(周贤明), Jing Wei(尉静), Rui Cheng(程锐), Yan-Hong Chen(陈燕红), Ce-Xiang Mei(梅策香), Li-Xia Zeng(曾利霞), Chang-Hui Liang(梁昌慧), Yao-Zong Li(李耀宗), Yong-Tao Zhao(赵永涛), and Xiao-An Zhang(张小安)

Citation: Chin. Phys. B, 2021, 30 (**8**): 083201. DOI: 10.1088/1674-1056/abe22f
Journal homepage: http://cpb.iphy.ac.cn; http://iopscience.iop.org/cpb

What follows is a list of articles you may be interested in

Molecular photoelectron momentum and angular distributions of N_2 molecules by ultrashort attosecond laser pulses

Si-Qi Zhang(张思琪), Qi Zhen(甄琪), Zhi-Jie Yang(杨志杰), Jun Zhang(张军), Ai-Hua Liu(刘爱华), Kai-Jun Yuan(元凯军), Xue-Shen Liu(刘学深), and Jing Guo(郭静)

Chin. Phys. B, 2021, 30 (**4**): 043201. DOI: 10.1088/1674-1056/abca22

Charge-state populations for the neon-XFEL system

Ping Deng(邓萍), Gang Jiang(蒋刚)

Chin. Phys. B, 2019, 28 (**6**): 063203. DOI: 10.1088/1674-1056/28/6/063203

Extreme ultraviolet and soft x-ray spectral lines in Rb XXIX

Indu Khatri, Arun Goyal, Sunny Aggarwal, A K Singh, Man Mohan

Chin. Phys. B, 2016, 25 (**3**): 033201. DOI: 10.1088/1674-1056/25/3/033201

Extreme ultraviolet and x-ray transition wavelengths in Rb XXIV

Indu Khatri, Arun Goyal, Sunny Aggarwal, A. K. Singh, Man Mohan

Chin. Phys. B, 2015, 24 (**10**): 103202. DOI: 10.1088/1674-1056/24/10/103202

Broadband time-resolved elliptical crystal spectrometer for X-ray spectroscopic measurements in laser-produced plasmas

Wang Rui-Rong, Jia Guo, Fang Zhi-Heng, Wang Wei, Meng Xiang-Fu, Xie Zhi-Yong, Zhang Fan

Chin. Phys. B, 2014, 23 (**11**): 113201. DOI: 10.1088/1674-1056/23/11/113201

X-ray emission for Ar^{11+} ions impacting on various targets in the collisions near the Bohr velocity*

Xian-Ming Zhou(周贤明)[1,2], Jing Wei(尉静)[1], Rui Cheng(程锐)[3,†], Yan-Hong Chen(陈燕红)[3], Ce-Xiang Mei(梅策香)[1], Li-Xia Zeng(曾利霞)[1], Chang-Hui Liang(梁昌慧)[1], Yao-Zong Li(李耀宗)[1], Yong-Tao Zhao(赵永涛)[2,3], and Xiao-An Zhang(张小安)[1,3,‡]

[1] *Ion Beam and Optical Physics Joint Laboratory of Xianyang Normal University and Institute of Modern Physics of CAS, Xianyang Normal University, Xianyang* 712000, *China*

[2] *School of Science, Xi'an Jiaotong University, Xi'an* 710049, *China*

[3] *Institute of Modern Physics, Chinese Academy of Sciences, Lanzhou* 730000, *China*

(Received 15 December 2020; revised manuscript received 29 January 2021; accepted manuscript online 2 February 2021)

X-ray emission from the collisions of 3 MeV Ar^{11+} ions with V, Fe, Co, Ni, Cu, and Zn is investigated. Both the x-rays of the target atom and projectile are observed simultaneously. The x-ray yield is extracted from the original count. The inner-shell ionization cross section is estimated by the binary encounter approximation model and compared with the experimental result. The remarkable result is that the Ar *K*-shell x-ray yield is diminished with the target atomic number increasing, which is completely opposite to the theoretical calculation. That is interpreted by the competitive consumption of the energy loss for the ionization of inner-shell electrons between the projectile and target atom.

Keywords: ion–atom collision, near Bohr velocity, x-ray, coulomb ionization

PACS: 32.80.Aa, 32.30.Rj, 34.80.Dp, 79.20.Rf **DOI:** 10.1088/1674-1056/abe22f

1. Introduction

Compared to singly charged ions, the highly charged heavy ions (HCIs) have many advantages, such as strong electric field and high potential energy. It will deposit most of its energy in nanoscale range in the time scale of femtoseconds, during the interaction with solid target. This results in increasing radiation, enhanced ion sputtering, surface nanoscale defects, etc.[1–4] Investigating such collisions not only has significance for basic research such as astrophysics and atomic physics under extreme conditions, but also has important practical applications in life sciences, materials science, new energy technology and other fields.[5–8]

In inelastic collisions of HCI with target atoms, HCIs will release most of their energy in the form of electronic energy loss, and will give rise to the inner-shell ionization. Correspondingly, vacancies will be filled by radiating x-ray or emitting Auger electrons. Compared to electron, the x-ray has a greater attenuation length in the solid target and no energy change under the interaction with target. Thus, research of x-ray emission can provide an important method for atomic physics studies and trace element analyses.[9,10]

For a low energy HCI with velocity less than Bohr velocity, the kinetic energy is too small to ionize the inner-shell electrons, the main result of the interaction with solid surface is the neutralization of the projectile by electron capture from the target atoms. That has been studied experimentally by measuring the high resolution x-ray spectra, and can be well described by the classical over-barrier (COB) model.[11–16] For fast heavy ions with energies greater than a few tens of MeV/u, the time, in which the projectile passes through the target with the distance of characteristic x-ray attenuation length, is usually less than that of de-excitation for inner-shell vacancies which may be re-produced by multiple collisions due to the high energy. Therefore, the evolution of the projectile could not be observed by radiation measurement, and it mainly provides the information for the inner-shell ionization of target atoms. That has been extensively researched in experiment.[17–21] Moreover, many models have been developed to simulate such a process, such as binary encounter approximation (BEA),[22] plane wave born approximation (PWBA) and ECPSSR for coulomb ionization,[23–26] quasi molecular-orbital (MO) for electron promotion,[27,28] electron capture (EC) for charge transfer.[29,30]

However, in the energy region near the Bohr velocity, the projected range of the incident ions is generally less than 1 μm, which is much smaller than the attenuation length of characteristic x-rays. The inner-shell process of projectile and target atoms can be observed simultaneously. Due to the limitation

*Project supported by the National Key R&D Program of China (Grant No. 2017YFA0402300), the National Natural Science Foundation of China (Grant Nos. 11505248, 11775042, 11875096, and 11605147) the Scientific Research Program Funded by Shaanxi Provincial Education Department, China (Grant No. 20JK0975), the Scientific Research Plan of Science and Technology Department of Shaanxi Province, China (Grant Nos. 2021JQ-812 and 2020JM-624), Open Funds of MOE Key Laboratory of Material Physics and Chemistry under Extraordinary Conditions (Grant No. MPCEC201901), and Xianyang Normal University Science Foundation (Grant Nos. XSYK20009 and XSYK20024).

†Corresponding author. E-mail: chengrui@impcas.ac.cn

‡Corresponding author. E-mail: zhangxiaoan2000@126.com

© 2021 Chinese Physical Society and IOP Publishing Ltd

of experimental conditions, although a few works have been carried out to study separately the x-ray emission from projectile or target atoms,[31–38] the research investigating simultaneously the two phenomena is rare. It is also unclear for the correlation between the x-ray emission from projectile and target atoms, which respect to the distribution of energy loss between the projectile and target atoms. Here, we would like to explore such a relevance and present our recent experiment about the x-ray emission from the projectile and target atoms produced by the collisions near the Bohr velocity.

In the present work, the x-rays of the target atoms (V, Fe, Co, Ni, Cu, and Zn) and argon ions were measured as a function of the target atomic number. The experimental x-ray yields are compared with the theoretical calculations. Competition between these two emissions is discussed

2. Experimental method

The measurements have been carried out at the 320 kV high voltage experimental platform in Institute of Modern Physics, Chinese Academy of Sciences (IMP, CAS), Lanzhou, China. More details of the experimental system have been described in the previous work.[39,40] In brief, the ions are produced and extracted from the electron cyclotron resonance (ECR) ion source and selected by a 90° analyzing magnet, and then introduced into the ultrahigh vacuum target chamber (10^{-8} mbar) after acceleration, focus, multi-deflections and multi-collimations. The divergence of the beam is smaller than 0.2°. The ion beam impacts perpendicularly onto the target with a spot size of about Φ3 mm. In order to ensure single collision, the current intensity of ion beam is regulated and controlled in the magnitude of only a few of nA. The target, having a purity of 99.99 % with surface area of 15×20 mm^2 and thickness of 0.1 mm, is positioned on a sample holder. It permitted a three-dimensional movement to change the target position freely and removes away from the beam line in order to measure the current.

The emitted x-rays are detected by a silicon drift detector (SDD), which has an effective detection area of 7 mm^2 and a 12.5 μm beryllium window in the front of the detector. The SDD is placed at 80 mm far away from the target surface in the chamber and at 135° to the beam direction. The detector has an effective energy range of 0.5–14.3 keV when the gain was selected to be 100, and an energy resolution of about 136 eV at 5.9 keV. The energy calibration is carried out using simultaneously the two standard radioactive sources of ^{55}Fe and ^{241}Am, and then tested by measuring the K-shell x-rays of Al, V and Fe produced by photon irradiation. In this way, a precise measurement on the x-ray energy can be guaranteed. The SDD intrinsic efficiency, which combines the effects of transmission through the Beryllium window and interaction in the silicon detector, is well determined by transmission measurement.

The number of incident projectiles, which could not be measured immediately by recording the target current due to the influence of the secondary electron emission, is detected indirectly by the combined use of a penetrable Faraday cup and a common one. Before every measurement, the projectile numbers are detected by the penetrable Faraday cup (N_1) before the target and the common Faraday cup (N_2) after the target are recorded. The ration (R) of N_2/N_1 is checked. During the x-ray detection, the projectile number detected by the penetrable Faraday cup (N_1') is recorded. Therefore, the number of the projectile impacting on the target (N) can be calculated by the formula $N = N_1' \cdot R$.

3. Results and discussion

3.1. The typical x-ray from the interaction of Ar^{11+} ions with various targets

Figure 1 presents the typical x-ray spectra for 3 MeV Ar^{11+} ions impacting on V, Fe, Co Ni, Cu and Zn targets. This includes both x-rays of target atom and projectile. Due to the absorption of Be window for SDD, the L-shell x-rays of V and Ar are not observed in this experiment. According to the rough estimation of the BEA model, the K-shell x-ray production cross section of those targets is about 5 orders of magnitude smaller than that of the L-shell. In fact, the K-shell x-ray yield is too low to be measured. Thus, the target's K-shell x-rays are neglected. The line with the peak energy less than or about 1 keV is the L-shell x-ray of target atom.[41,42] The obvious tail at the high energy side of those L x-rays is mainly from the contribution of L-edge lines.

The two lines with energy about 3 keV are regarded as the K_α and K_β x-rays of Ar, which result from the transition of L- and M-shell electrons to K-shell vacancy, respectively.[41] For Ar^{11+} ions, in which the remaining orbital electron arrangement is $1s^2 2s^2 2p^3$, there is no K-shell hole. Thus, this x-ray is mainly from the decay of the second hollow atom (HA) below the surface. In brief, the recorded spectral lines are mainly the L-shell x-ray of target and the K-shell x-ray of projectile. Those come from the decay of inner-shell vacancies produced by the close collisions inside the target.

3.2. X-ray from the projectile

In Fig. 1, the spectra were normalized by the number of projectile, and one can find that, with the same incident ions, the relative intensity of Ar K-shell x-ray is decreased with the increase of target atomic number. Furthermore, the x-ray yield per incident ion was obtained from the counts using the following formula:[40]

$$Y = \frac{N_x}{N_p \eta \, (\Omega/4\pi)}. \tag{1}$$

Here, N_x is the x-ray counts recorded by SDD; N_p is the number of incident ions; η is the detection efficiency of the SDD;

Ω is the solid angle of the detector, which is about 0.0011 Sr in the present work. The principal uncertainties for the experimental data mainly result from x-ray count statistic (about 5%), incident ions recording (about 3%), detector efficiency (about 5%), and solid angle calculating (about 2%). The maximal uncertainty of the yield is about 8% after delivery.

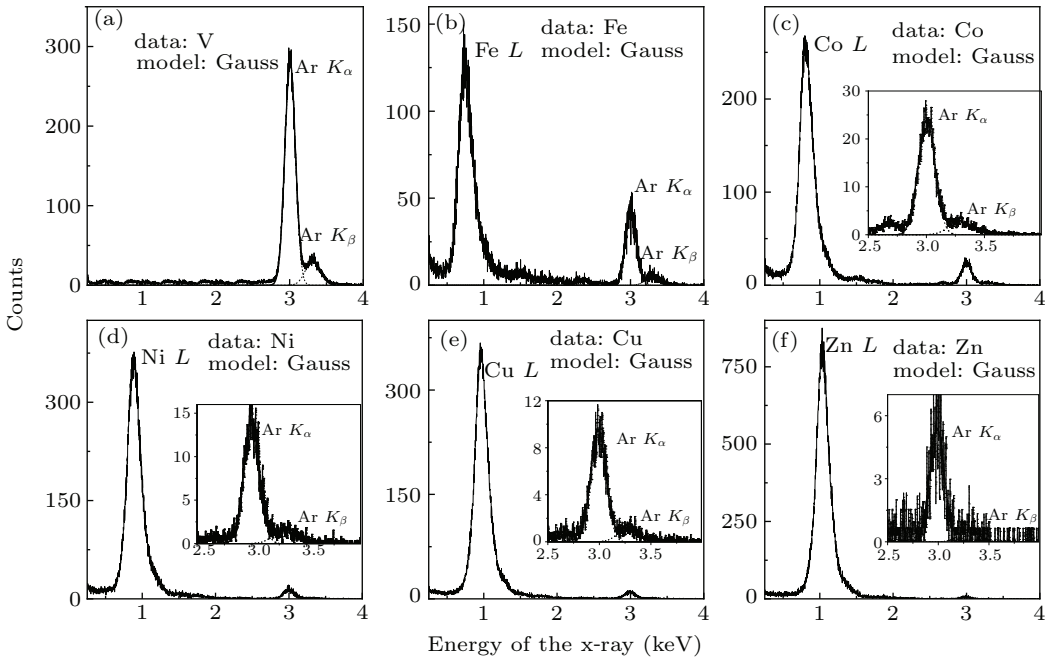


Fig. 1. Typical x-ray spectra for Ar^{11+} ions impacting on (a) V, (b) Fe, (c) Co, (d) Ni, (e) Cu and (f) Zn targets.

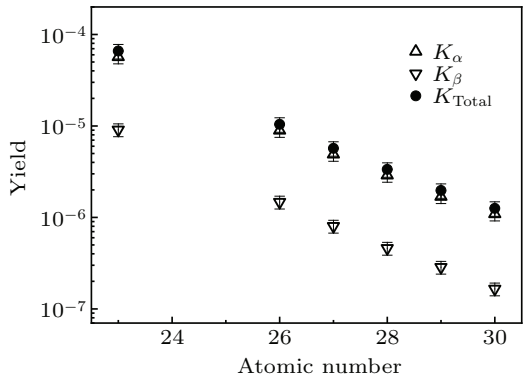


Fig. 2. Experimental yield of Ar K x-ray as a function of target atomic number.

The data of yield is extracted directly from the counts for K_α and K_β x-rays with the help of Eq. (1), and that of the K_{total} is the summation of those two data. They are all displayed in Fig. 2. The yield of K_α is roughly over that of K_β by a factor of about one order of magnitude. It is at the magnitude of about 10^{-4}–10^{-5} for K_α, and 10^{-5}–10^{-6} for K_β. It is obvious that the yield is decreased as a function of the target atomic number. Generally, the x-ray yield is positively related to the x-ray production cross section. According to the conversion formula $\sigma_{\text{x}} = \sigma_{\text{i}} \cdot \omega$ (σ_{x} is the x-ray production cross section,[43] σ_{i} is the ionization cross section, ω is the fluorescence yield), the x-ray production cross section is directly proportional to the ionization cross section. Thus, x-ray yield is usually positively related to the corresponding ionization cross section of inner-shell electrons. However, the present results indicate that the K-shell ionization cross section of Ar ions is diminished with the target atomic number.

Although the Ar L-shell x-rays were not observed in the present work, the ionization of L-shell electrons can be deduced from the K-shell x-ray emission. In the previous work,[44] we investigated the characteristic of Ar K-shell x-ray. As shown in Figs. 5 and 6 in Ref. [44], it was found that the x-ray energy of Ar K_α and K_β and the relative intensity ratio of K_β to K_α are all dwindled along with the target atomic number. This means that the multiple-ionization degree of L-shell decreases with the increase of target atomic number. This result indicates that the Ar L-shell ionization cross section is also diminished as a function of the target atomic number, and this is similar to that of K-shell.

The existing researches show that the inner-shell ionization produced by collisions near the Bohr velocity can be simulated by the BEA model.[45,46] The ionized orbital electrons can be regarded as free electrons, and the ionization cross section can be determined by the transferred energy and the velocity distribution of the 'free' electrons. For the same orbital electrons, if the projectile's velocity is constant, the ionization cross section is proportional to the nuclear charge of incident ions. Here, if we take the Ar^{11+} ion as the 'target atom' and the target atom as 'projectile', the incident velocities of the 'projectiles' are the same for the given 3 MeV kinetic energy. Therefore, the K and L-shell ionization cross section of Ar atom or ion is only related to the target atomic number. It increases with the target atomic number increasing, as shown in

Fig. 3. However, it is fascinating that the experimental result is exactly opposite to the theoretical estimation. It is proposed that it originates from the competition of the kinetic energy consumption between the inner-shell ionization of target atom and projectile. To verify this, the x-ray from target atom is also discussed in the following.

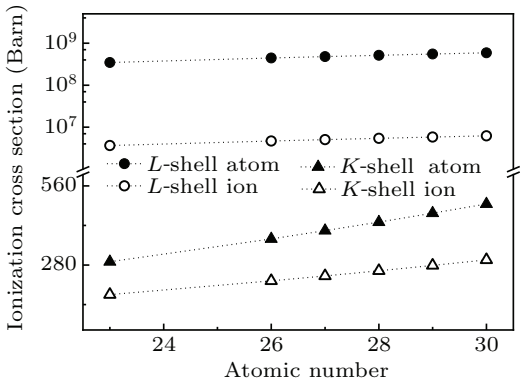


Fig. 3. Theoretical ionization cross section of K- and L-shell electrons for Ar atom and Ar^{11+} ion as a function of target atomic number.

3.3. X-ray from the target atoms

Figure 4 shows the theoretical L-shell x-ray production cross section of target atom ($Z_2 = 23$, 26, 27, 28, 29 and 30) produced by 3 MeV Ar^{11+} ions by using the BEA model. It is obvious that the cross section is gradually decreased with the increasing target atomic number. It goes without saying, because the ionization cross section is inversely proportional to the binding energy of the ionized electron, for the same incident ion, according to the formula of BEA.[45,46] Here, with the increase of Z_2, the binding energy of L-shell electrons is increased. Correspondingly, the cross section is naturally diminished. For example, the average L-shell binding energies of V, Fe, Ni, Cu and Zn atoms are about 530, 730, 800, 875, 950 and 1040 eV, respectively. The estimated L-shell x-ray production cross section is reduced from 8.3×10^4 to 3.2×10^3 barn.

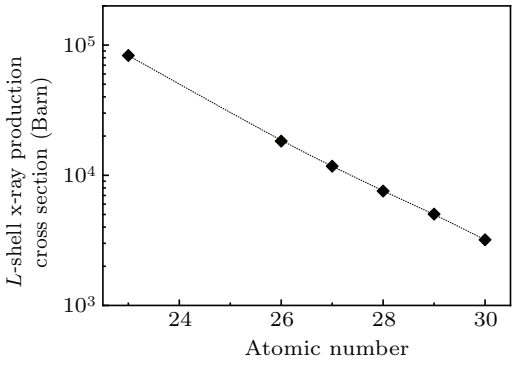


Fig. 4. Theoretical L-shell x-ray production cross section of target atom induced by 3 MeV Ar^{11+} ions.

Figure 5 gives the experimental L-shell x-ray yield of target atoms impacted by 3 MeV Ar^{11+}ions. It decreases from 2.28×10^{-3} to 8.32×10^{-4} for Z_2 from 26 to 30. It seems that it presents a similar trend with target atomic number as that of the theoretical calculations shown in Fig. 4. However, it is not true. In order to explain the problem conveniently, a simple normalization process is performed such that the theoretical simulation just can predict the experimental results for Fe target. The comparison of the theoretical cross section with the experimental results is shown in Fig. 6. One can find that the ratio of theory to experiment is less than 1 for $Z_2 = 27$–30 and dwindled as a function of Z_2. It indicates that the ionization of target atom cannot be simply estimated by BEA, and the distribution of the transferred energy should be considered between the target and projectile during the above collisions.

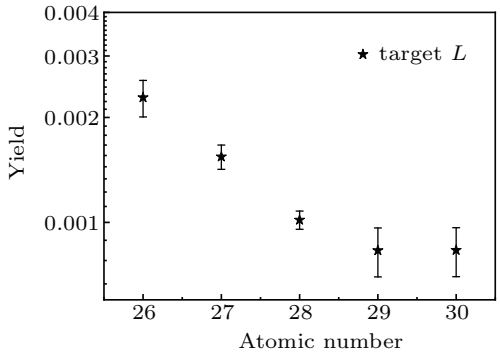


Fig. 5. Experimental L x-ray yield of target atom by 3 MeV Ar^{11+} ions impacting.

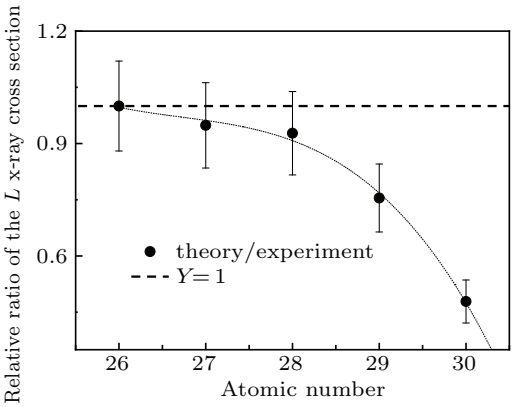


Fig. 6. The relative ratio of theory to experiment for target L x-ray production cross section by 3 MeV Ar^{11+} ions impacting.

3.4. Competition of the x-rays between projectile and target atom

Further, the x-ray yield of target atom is compared with that of projectile, as shown in Fig. 7. As the target atomic number increases, the ratio of x-ray yield of target atom to that of projectile is enhanced. It increases about 3.5 times for Z_2 from 26 to 30. This means that it is easier to excite the x-ray of target atom during the present collisions, and it has a greater increase compared with that of projectile.

Considering the results of Figs. 2–7, it is proposed that during the interaction of 3 MeV Ar^{11+} ions with the experimental targets, the projectile loses its kinetic energy by coulomb collisions, which results in the inner-shell ionization

of target atom and itself. There is a competition between such two ionizations. With the increase of target atomic number, the proportion of the transferred energy used to ionize the target atom is enlarged, correspondingly, that for projectile is dwindled. As a result, for the projectile of Ar, the K-shell ionization is decreased, and the degree of the multiple ionization for the L-shell is diminished. That leads to the dwindled yield and blue shift of energy for K x-ray, and the diminution of relative intensity ration of K_β to K_α.

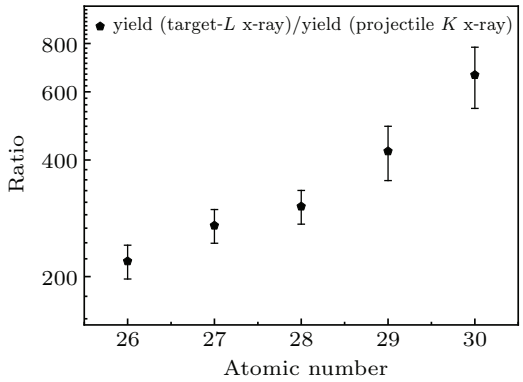


Fig. 7. The experimental ratio of target x-ray yield to that of projectile as a function of target atomic number.

4. Conclusion and perspectives

The x-rays of target atom and projectile are investigated completely for 3 MeV Ar^{11+} ions impacting on V, Fe, Co, Ni, Cu and Zn targets. The results indicate that, during the collision of highly charged heavy ions with solid target in the energy region near the Bohr velocity, the inner-shell electrons of target atom and incident ions can both be ionized by coulomb interaction. There is a competition for the consumption of transferred energy between the above ionization. The most important result is that the distribution of incident energy used to ionize the projectile is reduced, with the increase of target atomic number. This leads to the remarkable result that the experimental K-shell x-ray yield of Ar ions is diminished.

Acknowledgment

The authors sincerely acknowledge the technical supports from the group of 320 kV HCI platform.

References

[1] Littmark U and Sigmund P 1975 *J. Phys. D* **8** 241
[2] Ciricosta O, Vinkoe S M, Chung H K, Cho B I, Brown C R D, Burian T, Chalupský J, Engelhorn K, Falcone RW, Graves C, Hájková V Higginbotham A, Juha L, Krzywinski J, Lee H J, Messerschmidt M, Murphy C D, Ping Y, Rackstraw D S, Scherz A, Schlotter W, Toleikis S, Turner J J, Vysin L, Wang T, Wu B, Zastrau U, Zhu D, Lee R W, Heimann P, Nagler B and Wark J S 2012 *Phys. Rev. Lett.* **109** 065002
[3] Liedke B, Heinig K H and Möller W 2013 *Nucl. Instrum. Methods B* **316** 56
[4] Schenkel T, Hamza A V, Barnes A V and Schneider D H 1999 *Prog. Surf. Sci.* **61** 23
[5] Wilhelm R A, Gruber E, Schwestka J, Kozubek R, Madeira T I Marques J P Kobus J, Krasheninnikov A V, Schleberger M and Aumayr F 2017 *Phys. Rev. Lett.* **119** 103401
[6] Siddique N, Waheed S, Daud M, Markwitz A and Hopke P K 2012 *J. Radioanal. Nucl. Chem.* **293** 351
[7] Zeng L X, Zhou X M, Cheng R, Wang X, Ren J R, Lei Y, Ma L D, Zhao Y T, Zhang X A and Xu Z F 2017 *Sci. Rep.* **7** 06891
[8] Guo Y P, Yang Z H, Hu B T, Wang X, Song Z Y, Xu Q M, Zhang B M, Chen J, Yang B and Yang J 2016 *Sci. Rep.* **6** 30644
[9] Miranda J, Luciob O G and Lugo-Licona M F 2007 *Rev. Mex. Fis.* **53** 29
[10] Siddique N, Waheed S, Daud M, Markwitz A and Hopke P K 2012 *J. Radioanal. Nucl. Chem.* **293** 351
[11] Briand J P, Billy L, Charles P and Essabaa S, Briand P, Geller R, Desclaux J P, Bliman S and Ristor C 1990 *Phys. Rev. Lett.* **65** 159
[12] Schmidt-Böcking H, Schulz M, Cocke C L, Hagmann S and Stöckli M 1991 *Phys. Rev. A* **44** 1653
[13] Briand J P, Billy L, Charles P and Essabaa S, Briand P, Geller R, Desclaux J P, Bliman S and Ristori C 1991 *Phys. Rev. A* **43** 565
[14] Briand J P, Thuriez S, Giardino G, Borsoni G, Froment M, Eddrief M and Sébenne C 1996 *Phys. Rev. Lett.* **77** 1452
[15] Briand J P, Giardino G, Borsoni G, Froment M, Eddrief M, Sébenne C, Bardin S and Schneider D, Jin J, Khemliche H, Xie Z and Prior M 1996 *Phys. Rev. A* **54** 4136
[16] Burgdörfer J, Lerner P and Meyer F W 1991 *Phys. Rev. A* **44** 5674
[17] Garcia J D, Fortner R J and Kavanagh T M 1973 *Rev. Mod. Phys.* **45** 111
[18] Reyes-Herrera J and Miranda J 2009 *Nucl. Instrum. Methods B* **267** 1767
[19] Lapicki G 2009 *J. Phys. B: At. Mol. Opt. Phys.* **42** 145204
[20] Mitra D, Sarkar M, Bhattacharya D, Santra S, Mandal A C and Lapicki G 2010 *Nucl. Instrum. Methods B* **268** 450
[21] Kumar A, Agnihotri A N, Chatterjee S, Kasthurirangan S, Misra D, Choudhury R K, Sarkadi L and Tribedi L C 1991 *Phys. Rev. A* **81** 062709
[22] Gryzinski M 1965 *Phys. Rev.* **138** A336
[23] Johnson D E, Basbas G and McDaniel F D 1979 *At. Data Nucl. Data Tables* **24** 1
[24] Brandt W and Lapicki G 1981 *Phys. Rev. A* **23** 1717
[25] Liu Z and Cipolla S J 1996 *Comput. Phys. Commun.* **97** 315
[26] Lapicki G 2002 *Nucl. Instrum. Methods B* **189** 8
[27] Barat M and Lichten W 1972 *Phys. Rev. A* **6** 211
[28] McGuire J H and Richard P 1973 *Phys. Rev. A* **8** 1374
[29] Lapicki G and Losonsky W 1977 *Phys. Rev. A* **15** 896
[30] Lapicki G and Losonsky W 1979 *Phys. Rev. A* **20** 481
[31] Ding X B, Wu C Q, Cao M X, Zhang D H, Zhang M W, Xue Y L, Yu D Y and Dong C Z 2020 *Chin. Phys. B* **29** 033101
[32] Zhou X M, Cheng R, Lei Y, Sun Y B, Wang Y Y, Wang X, Xu G, Mei C X, Zhang X A, Chen X M, Xiao G Q and Zhao Y T 2016 *Chin. Phys. B* **25** 023402
[33] Ismail A S, Dong C Z, Wang X L, Zhou W D and Wu Z W 2014 *Chin. Phys. B* **23** 023101
[34] Liu Y, Xu Z F, Wang X, Zeng L X and Liu T 2020 *Acta Phys. Sin.* **69** 043201 (in Chinese)
[35] Liang C H, Zhang X A, Li Y Z, Zhao Y T, Zhou X M, Wang X, Mei C X and Xiao G Q 2018 *Acta Phys. Sin.* **67** 243201 (in Chinese)
[36] Mei C X, Zhang X A, Zhou X M, Zhao Y T, Ren J R, Wang X, Lei Y, Sun Y B, Cheng R, Xu G and Zeng L X 2017 *Acta Phys. Sin.* **66** 143401 (in Chinese)
[37] Zhang X A, Mei C X, Zhang Y, Zhao Y T, Xu Z F, Zhou X M, Ren J R, Cheng R, Liang C H, Li Y Z, Zeng L X, Yang Z H, Chen X M, Li F L and Xiao G Q 2016 *Sci. Sin.-Phys. Mech. Astron.* **46** 073006
[38] He B, Liu C L, Yan J, Wang J G and Ning Y 2005 *Acta Phys. Sin.* **54** 3075 (in Chinese)
[39] Zhou X M, Cheng R, Zhao Y T, Lei Y, Chen Y H, Chen X M, Wang YY, Ma X W and Xiao G Q 2018 *Nucl. Instrum. Methods B* **416** 94
[40] Zhou X M, Zhao Y T, Cheng R, Wang Y Y, Lei Y, Wang X and Sun Y B 2013 *Nucl. Instrum. Methods B* **299** 61
[41] X-ray data book: http://xdb.lbl.gov/, 2nd edn, January 2001
[42] Bearden J A 1967 *Rev. Mod. Phys.* **39** 78
[43] Krause M O 1979 *J. Phys. Chem. Ref. Data* **8** 307)
[44] Zhou X M, Cheng R, Wang Y Y, Lei Y, Chen Y H, Ma X W, Xiao G Q and Zhao Y T 2017 *Sci. Rep.* **9** 5359
[45] Zhou X M, Cheng R, Lei Y, Liu S D, Deng J C, Sun Y B, Ren J R Wang Y Y, Zhao Y T and Xiao G Q 2014 *Nucl. Instrum. Methods B* **340** 11
[46] Zhou X M, Zhao Y T, Ren J R, Cheng R, Lei Y, Sun Y B, Xe G, Wang Y, Liu S D and Xiao G Q 2013 *Chin. Phys. B* **22** 113402